Aeromagnetic 3D subsurface imaging in the Otoge Cauldron, Shitara area, Central Japan

Tadashi Nakatsuka[(1)], and Shigeo Okuma[(1)]

[(1)] *Geological Survey of Japan, AIST (tad.nktk@ni.aist.go.jp)*

ABSTRACT

We have developed an aeromagnetic 3D subsurface imaging software applicable to helicopter-borne magnetic (total force) surveys in mountainous regions, based on the compact regularization to constrain source magnetization. The method accepts the surface undulation and variable thickness slicing of model layers, and the regularization criterion of minimum effective source volume is adopted. First, the algorithms were applied to simple synthetic models and some geologic models to examine the efficiency of the method. The results revealed a good recovery of subsurface image in spite of the intrinsic difficulty of the non-unique problem, and it was proven that the compact regularization is useful to interpret magnetic anomaly data in terms of 3D source configuration.

The helicopter-borne magnetic survey data in the Shitara area was put into analysis by this 3D imaging software. The geology of Shitara area is characterized by middle Miocene Otoge and Shitara igneous complexes, the Otoge Cauldron structure with stock, and post-cauldron intrusions of dike swarms (Otoge cone sheets and Shitara central dike swarm). The 3D imaging analysis of magnetic anomalies revealed the magnetization structure (to the depth of 3000m) of the magma reservoir of Otoge Cauldron, the Otoge cone sheets, and Otoge stock, to be consistent with existing studies from surface geology.

KEY WORDS: aeromagnetic anomaly, 3D imaging, Shitara, Otoge Cauldron, compact inversion, effective volume minimization

INTRODUCTION

Recent developments in aeromagnetic surveying, including improved accuracy of position fixing and navigation, have enabled us to detect more details of subsurface structure. High-resolution aeromagnetic survey using a helicopter has become more popular especially in areas of volcanic activities. Magnetic survey flights by helicopters are usually parallel to the topographic surface, but the altitudes of observation may be too variable to be regarded as a smooth surface. The procedure in use of the equivalent source technique was proven to give efficient way of altitude reduction (Nakatsuka and Okuma, 2006a).

As for the interpretation of magnetic anomalies in terms of subsurface magnetic structure, we often used the method of magnetization intensity (2D) mapping (Okuma *et al*., 1994; Nakatsuka, 1995; Okubo *et al*., 2005), but the technology of 3D imaging is straight forward of it. As is well known, the magnetic (potential field) anomaly data cannot give a unique solution of the subsurface structure theoretically, and there are infinite possibilities of equivalent 3D sources. So, some constraint on the source distribution is necessary to get valid result, and the result should be inspected for its plausibility. Unless another kind of observation is available for the unified interpretation of multi discipline data, some philosophical strategy should be given to overcome the difficulty.

The earth science can be regarded as the knowledge of the nature by simplifying the complicated situation and the diversity. Minimum norm solution will be one candidate, and was effective for underdetermined solution of the magnetization intensity mapping. In the simple synthetic study of 3D imaging, however, it was proven that minimum norm criterion cannot give a focused image of subsurface structure, but tends to result in a broader shape of source with vague boundary especially towards deeper side as an equivalent source model (Nakatsuka and Okuma, 2006b). The selection of smoothness (minimum roughness) regularization, as often used in non-linear problem such as in EM methods (e.g., Uchida, 1993), seems to have similar character. Now we adopt the compactness criterion to get a localized source image from the observation (Nakatsuka and Okuma, 2009), as was developed by Last and Kubik (1983), and Portniaguine and Zhdanov (2002).

3D IMAGING

As we are aiming for the application of 3D imaging to aeromagnetic surveys in mountainous regions such as active volcanoes, our model configuration permits surface undulation and variable depth slicing of source layers as shown in Fig. 1. There are two options to define model configuration, (a) horizontal layer slicing, or (b) constant burial depth slicing. Here we introduced the additional source zone around the area of observation to avoid edge effect (Nakatsuka and Okuma, 2006a). As the analysis result in this zone of

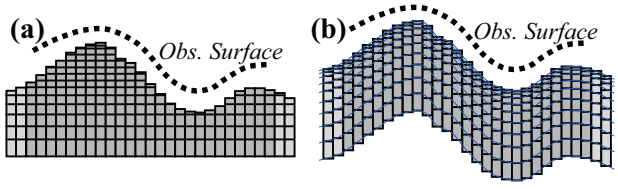

Figure 1. Two types of layer configuration (section view) for 3D magnetization imaging software.

surrounding sources (away from observation) is not very reliable, usually we exclude them in the result illustration.

The basic formula of 3D subsurface imaging is completely the same as the equivalent source analysis or the magnetization intensity mapping, but the sources are distributed in three-dimensional space and have the physical quantity of magnetization. Here we deal with a model of invariant direction of magnetization, because too loose constraint on the physical situation in the underdetermined problem may result in an impractical extreme solution.

The magnetic anomaly $f(\boldsymbol{p})$ at the observation point $\boldsymbol{p}$ is expressed as

$$f(\boldsymbol{p}) = \int_Q A(\boldsymbol{p},\boldsymbol{q})\, s(\boldsymbol{q})\, ds\,, \qquad (1)$$

where $s(\boldsymbol{q})$ is the magnetization of the source located at $\boldsymbol{q}$, and $A(\boldsymbol{p}, \boldsymbol{q})$ is the source effect coefficient (geometric factor) combining $f(\boldsymbol{p})$ with $s(\boldsymbol{q})$. First, we solved the equation (1) by the conjugate gradient (CG) method. The CG method applied to underdetermined linear problem gives a minimum norm solution, but the result from the simple CG solution could not give a focused image of subsurface structure (Nakatsuka and Okuma, 2006b). As a solution for such problem, various methods of regularization are utilized. The generalized formulation for them is given as follows.

Using a vector/matrix notation, discretized form of the original equation (1) can be expressed as

$$\boldsymbol{f} = \mathbf{A}\boldsymbol{s}\,, \qquad (2)$$

and the simple CG method searches for the condition

$$(\boldsymbol{f} - \mathbf{A}\boldsymbol{s})^{\mathrm{T}}(\boldsymbol{f} - \mathbf{A}\boldsymbol{s}) \;\rightarrow\; \mathrm{Min}\,, \qquad (3)$$

which corresponds to the normal equation,

$$\mathbf{A}^{\mathrm{T}}\boldsymbol{f} = \mathbf{A}^{\mathrm{T}}\mathbf{A}\boldsymbol{s}\ . \qquad (4)$$

In case of the regularization methods, another term is added in the minimizing functional as

$$(\boldsymbol{f} - \mathbf{A}\boldsymbol{s})^{\mathbf{T}}(\boldsymbol{f} - \mathbf{A}\boldsymbol{s}) + e(\mathbf{B}\boldsymbol{s})^{\mathbf{T}}(\mathbf{B}\boldsymbol{s}) \rightarrow \mathbf{Min}\,, \qquad (5)$$

where $\mathbf{B}$ is the penalizing operator matrix, and e is a trade-off parameter to adjust the penalizing weight ratio between the misfit term and the regularization term. This formulation (5) corresponds to the normal equation for the combined equation

$$\begin{bmatrix} \mathbf{A} \\ \sqrt{e}\mathbf{B} \end{bmatrix} \boldsymbol{s} = \begin{bmatrix} \boldsymbol{f} \\ \mathbf{0} \end{bmatrix}, \qquad (6)$$

and the application of simple CG method to this

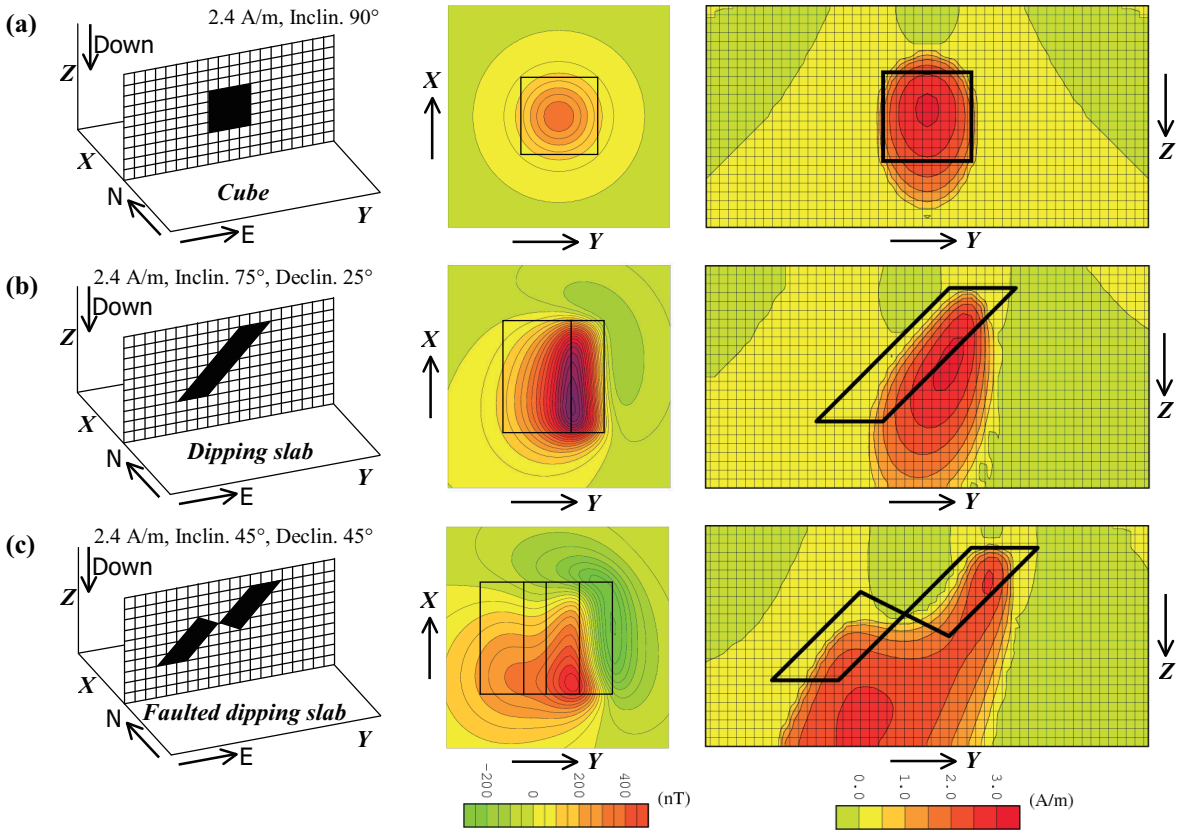

Figure 2. Synthetic example of 3D imaging for the models of (a) cube, (b) dipping slab, and (c) faulted dipping slab, as similar to those discussed by Portniaguine and Zhdanov (2002) (after Nakatsuka and Okuma (2009)).
Left: sketch of source body at the E-W vertical section; Center: synthetic magnetic anomaly (calculated for the magnetization and geomagnetic field direction parameters described in the left panel) with horizontal outline of source body; Right: result of compact inversion (imaging by minimum effective volume regularization) at the E-W vertical section crossing the center of the source body. For each model, the synthetic magnetic anomaly distribution (center panel) was regarded as the observation and was put into the process to obtain 3D image of subsurface magnetization, only one typical section of which is illustrated on the right panel. These analyses are based on the a priori knowledge of the magnetization direction but without any source intensity distribution of initial condition (starting from parameter values of all zeros).

equation is reduced to the regularized solution for the equation (2).

If a unit matrix is selected for **B**, the formulation (5) means the minimum norm regularization. Similarly, if **B** is Laplacian (roughness operator) matrix, the problem is reduced to the smooth inversion.

COMPACTNESS REGULARIZATION

Last and Kubik (1983) first introduced a compact inversion technique in a 2D gravity analysis, and Portniaguine and Zhdanov (2002) developed it in 3D magnetic imaging. The idea is to adopt the penalizing operator matrix as

$$\mathbf{B} = \mathrm{diag}\left\{1 \Big/ \sqrt{{s_i}^2 + \delta^2}\right\}, \qquad (7)$$

and the regularizing factor R of (5) becomes

$$R = (\mathbf{B}\boldsymbol{s})^{\mathrm{T}}(\mathbf{B}\boldsymbol{s}) = \sum_i \frac{{s_i}^2}{{s_i}^2 + \delta^2}. \qquad (8)$$

Here $\delta(>0)$ is a critical value of magnetization, where source bodies with small magnetization well below δ $(|s_i| << \delta)$ are regarded as ineffective to build the anomalies. As each element of R has a value between 0 $(|s_i| << \delta)$ and 1 $(|s_i| >> \delta)$, the minimization of R corresponds to the minimization of number of sources contributing the anomaly buildup. This is equivalent to minimizing source volume if source model is composed of equi-volume bodies. In case of the model composed of variable volume bodies, as we want to use, the penalizing operator and the regularizing factor should be

$$\mathbf{B} = \mathrm{diag}\left\{\sqrt{\frac{v_i}{{s_i}^2 + \delta^2}}\right\}, \qquad (9)$$

$$R = (\mathbf{B}\boldsymbol{s})^{\mathrm{T}}(\mathbf{B}\boldsymbol{s}) = \sum_i \frac{v_i\, {s_i}^2}{{s_i}^2 + \delta^2}, \qquad (10)$$

where v_i is the volume of i-th source body.

SYNTHETIC MODEL EXAMPLE

Next the algorithm of minimum effective volume regularization was applied to synthetic model examples. In Fig. 2, there are three models nearly same as those discussed by Portniaguine and Zhdanov (2002), and 71×71×25 source blocks including surrounding zone were assumed. The result is generally similar to theirs. Though the horizontal location is recovered well, the recovery of vertical structure is not so correct. This might indicates the limitation from the inherent non-uniqueness. Nevertheless the results of compact inversion methods can be informative to interpret magnetic anomalies in terms of 3D structure.

In the process of iterative solution of the problem, the trade-off parameter e plays an important role. To minimize misfit term, e is decreased during the process. However, if e is decreased too fast, the existence of regularization term becomes ineffective and the solution resembles the minimum norm one. To make

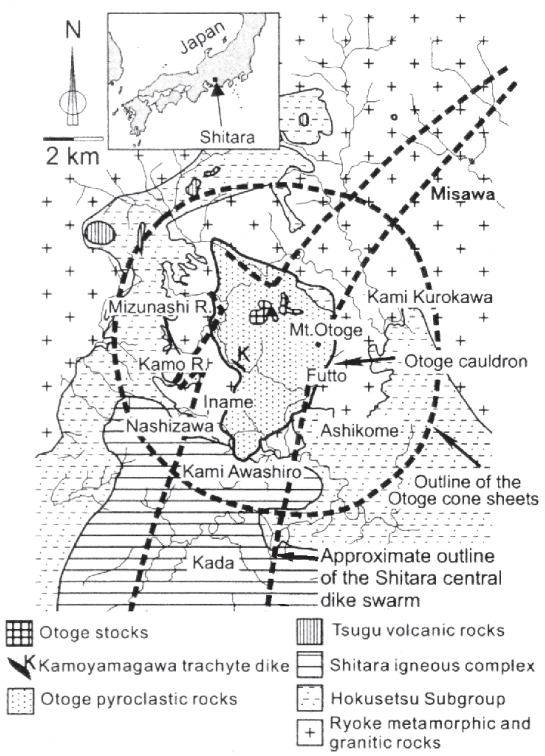

Figure 3. Outline of the geology of the Otoge volcanic complex after Takada (1987) and Geshi (2003).

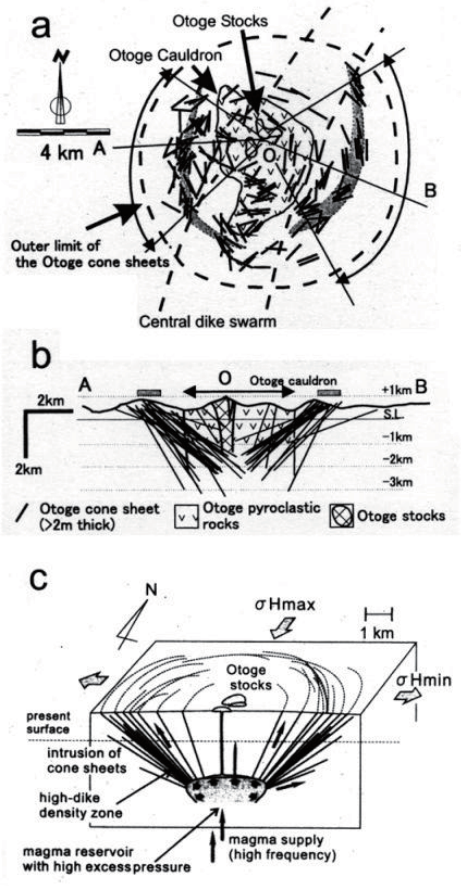

Figure 4. Distribution (a) and cross-section (b) of Otoge cone sheets, and their schematic model (c) after Geshi (2003, 2005).

sure the solution becomes compact, relatively large value of *e* should be maintained as long as possible.

OTOGE CAULDRON

There is a ring-shaped geological structure in the Shitara area, Central Japan. From the geological and petrological studies, Takada (1987) reported the structure of Middle Miocene Otoge volcanic complex with a cauldron structure and post-cauldron intrusions of dike and sheet swarms, and Geshi (2003, 2005) discussed the evolution of the structure. Figure 3 illustrates the geologic outline of the area. The volcanic activities of the Otoge igneous complex are divided into two stages, i.e., the cauldron-forming stage of the eruption of the Otoge pyroclastic rocks which filled the Otoge cauldron, and the post-cauldron stage of intrusions of Otoge cone sheets, Otoge stock, and Shitara central dike swarm. Among such geologic features, the distribution and the dip of Otoge cone sheets suggests the depth to the magma reservoir of post-cauldron activity (Fig. 4).

A helicopter-borne magnetic survey in this area was conducted in 2003, with a flying altitude of 300m above ground and a line-spacing of 500 m in use of a stinger-type sensor mount. Although only limited data was acquired to map rather small area (because this survey was aimed only at the verification of a newly developed equipment), a typical magnetic anomaly pattern for the ring structure was revealed.

This magnetic anomaly data was put into 3D imaging analysis of compact regularization after removing a linear regional trend. The 10 layers source model of constant burial depth slicing was used, and a total of about 13 thousands data (100m mesh) was used to estimate 16 times as many unknown parameters (including surrounding zone) as the observation. Here the magnetization direction same as the present geomagnetic field was assumed, but the starting model (initial guess) of the analysis is null source (all zero parameter values). The results of analysis are shown as the estimated magnetization distribution on each layer (Fig. 5d) and two vertical sections (Fig. 5e) along the blue lines on Fig. 5a.

CONCLUSION

The result of aeromagnetic 3D imaging analysis in Shitara area revealed a quite reasonable subsurface image of the magma reservoir, the Otoge cone sheets and Otoge stocks for the post-cauldron activity, as inferred from geological studies.

1) The principal magnetic feature of Otoge Cauldron is characterized by the post-cauldron magma reservoir at the depth of 2000m and below. Its shape is nearly a vertical cylinder with a diameter of about 5km.

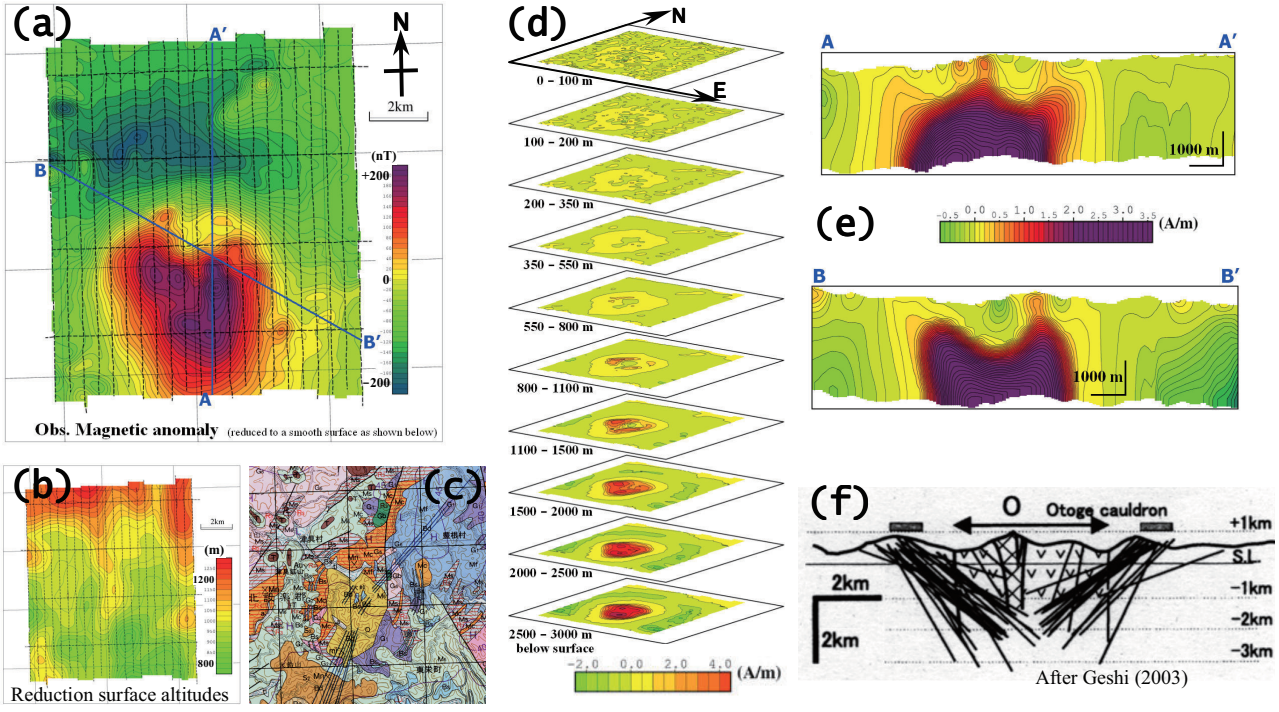

Figure 5. 3D imaging analysis of aeromagnetic anomalies in the Otoge Cauldron, Shitara area. Aeromagnetic anomaly (a) reduced to a smooth reduction surface (b) was put into 3D imaging process with the minimum effective source volume regularization. The result is shown as a magnetization distribution on each depth-range layer (d), and two vertical sections (e) along the blue lines A-A' and B-B' in (a). The geologic map of the area (c) (Makimoto *et al.*, 2004) and the cross section of Otoge cone sheets (f) (same as in Fig. 4) are shown for reference.

2) The shallower extension of magma reservoir branches into two parts (WNW and ESE) and the massive body rises up to the depth of 800m at the western branch. They seem to be related to the cone sheets activity with a non-axisymmetric distribution.

As the analysis was performed with the model of depth-range of 0-3000m, there is a possibility that the effect of actual magnetic structure deeper than 3000m may distort the analysis result especially in deeper portion.

REFERENCES

Geshi, N., 2003, Development of the Middle Miocene Otoge volcanic complex, Shitara district, central Japan. *J. Geol. Soc. Japan*, **109**, 580-594.

Geshi, N., 2005, Structural development of dike swarms controlled by the change of magma supply rate: the cone sheets and parallel dike swarms of Miocene Otoge igneous complex, Central Japan. *J. Volcanol. Geotherm. Res.*, **141**, 267-281. doi: 10.1016/j.jvolgeores.2004.11.002

Last, B. J. and K. Kubik, 1983, Compact gravity inversion. *Geophysics*, **48**, 713-721. doi: 10.1190/1.1441501

Makimoto, H., N. Yamada, K. Mizuno, A. Takada, M. Komazawa, and S. Sudo, 2004, *Geological Map of Japan 1:200,000 , Toyohashi and Irago Misaki*, Geol. Surv. Japan, AIST.

Nakatsuka, T., 1995, Minimum norm inversion of magnetic anomalies with application to aeromagnetic data in the Tanna area, Central Japan. *J. Geomag. Geoelectr.*, **47**, 295-311.

Nakatsuka, T. and S. Okuma, 2006a, Reduction of geomagnetic anomaly observations from helicopter surveys at varying elevations. *Explor. Geophys.* **37** ／ *Butsuri-Tansa (Geophys. Explor.)* **59** ／ *Mulli-Tamsa (Geophys. Explor.)* **9**, 121-128. doi: 10.1071/EG06121

Nakatsuka, T. and S. Okuma, 2006b, 3D subsurface imaging by aeromagnetic data. *Proc. 115th SEGJ Conference*, 196-199.

Nakatsuka, T. and S. Okuma, 2009, Aeromagnetic 3D subsurface imaging with source volume minimization. *Extended Abstracts, 9th SEGJ Intl. Stmp.*, 6, 4p.

Okubo, A., Y. Tanaka, M. Utsugi, N. Kitada, H. Shimizu, and T. Matsushima, 2005, Magnetization intensity mapping on Unzen Volcano, Japan, determined from high-resolution, low-altitude helicopter-borne aeromagnetic survey. *Earth Planets Space*, **57**, 743-753.

Okuma, S., M. Makino, and T. Nakatsuka, 1994, Magnetization intensity mapping in and around Izu-Oshima Volcano, Japan. *J. Geomag. Geoelectr.*, **46**, 541-556.

Portniaguine, O. and M. S. Zhdanov, 2002, 3-D magnetic inversion with data compression and image focusing. *Geophysics*, **67**, 1532-1541. doi: 10.1190/1.1512749

Takada, A., 1987, Structure of a cauldron in the Otoge Ring Complex, Shitara district, Aichi Prefecture, central Japan. *J. Geol. Soc. Japan*, **93**, 107-120.

Uchida, T., 1993, Smooth 2-D inversion for magnetotelluric data based on statistical criterion ABIC. *J. Geomag. Geoelectr.*, **45**, 841-858.